

Article

Solubility and Thermodynamic Analysis of Isotretinoin in Different (DMSO + Water) Mixtures

Faiyaz Shakeel ^{1,*}, Nazrul Haq ¹, Sultan Alshehri ¹, Miteb Alenazi ², Abdulrahman Alwhaibi ²
and Ibrahim A. Alsarra ¹

¹ Department of Pharmaceutics, College of Pharmacy, King Saud University, P.O. Box 2457, Riyadh 11451, Saudi Arabia; nhaq@ksu.edu.sa (N.H.); salshehri1@ksu.edu.sa (S.A.); ialsarra@ksu.edu.sa (I.A.A.)

² Department of Clinical Pharmacy, College of Pharmacy, King Saud University, P.O. Box 2457, Riyadh 11451, Saudi Arabia; mitalanazi@ksu.edu.sa (M.A.); aalwhaibi@ksu.edu.sa (A.A.)

* Correspondence: fsahmad@ksu.edu.sa

Abstract: The solubility and solution thermodynamics of isotretinoin (ITN) (3) in numerous {dimethyl sulfoxide (DMSO) (1) + water (H₂O) (2)} combinations were studied at 298.2–318.2 K under fixed atmospheric pressure of 101.1 kPa. A shake flask methodology was used to determine ITN solubility, and correlations were made using the “van’t Hoff, Apelblat, Buchowski-Ksiazczak λh , Yalkowsky-Roseman, Jouyban-Acree, and Jouyban-Acree-van’t Hoff models”. In mixtures of {(DMSO (1) + H₂O (2))}, the solubility of ITN in mole fractions was enhanced with the temperature and DMSO mass fraction. The mole fraction solubility of ITN was highest in neat DMSO (1.02×10^{-1} at 318.2 K) and lowest in pure H₂O (3.14×10^{-7} at 298.2 K). The output of computational models revealed good relationships between the solubility data from the experiments. The dissolution of ITN was “endothermic and entropy-driven” in all of the {(DMSO (1) + H₂O (2))} mixtures examined, according to the positive values of measured thermodynamic parameters. Enthalpy was discovered to be the driving force behind ITN solvation in {(DMSO (1) + H₂O (2))} combinations. ITN-DMSO displayed the highest molecular interactions when compared to ITN-H₂O. The outcomes of this study suggest that DMSO has a great potential for solubilizing ITN in H₂O.

Keywords: computational models; isotretinoin; molecular interactions; {DMSO (1) + water (2)} mixtures; solubility; thermodynamic analysis



Citation: Shakeel, F.; Haq, N.; Alshehri, S.; Alenazi, M.; Alwhaibi, A.; Alsarra, I.A. Solubility and Thermodynamic Analysis of Isotretinoin in Different (DMSO + Water) Mixtures. *Molecules* **2023**, *28*, 7110. <https://doi.org/10.3390/molecules28207110>

Academic Editors: Piotr Cysewski, Tomasz Jeliński and Maciej Przybyłek

Received: 7 September 2023

Revised: 9 October 2023

Accepted: 13 October 2023

Published: 16 October 2023



Copyright: © 2023 by the authors. Licensee MDPI, Basel, Switzerland. This article is an open access article distributed under the terms and conditions of the Creative Commons Attribution (CC BY) license (<https://creativecommons.org/licenses/by/4.0/>).

1. Introduction

The drug isotretinoin (ITN) is an isomer of retinoic acid, also referred to as 13-*cis*-retenoic acid, that has a *cis* structure [1,2]. Its molecular structure/formula is shown in Figure 1A [3]. ITN was shown to be suitable for the treatment of several malignancies because it plays a significant part in regulating gene expression [4,5]. Additionally, it was discovered to be effective in the treatment of several skin conditions, including psoriasis, skin cancer, and acne [6–10]. It is touted as the most effective treatment for acne [10,11]. A practical approach for the oral administration of ITN in pediatric neuroblastoma patients was recently reported [12] because the patients were unable to swallow marketed tablets or capsules. Due to its poor solubility in water and high lipophilicity, ITN presents challenges in the development of formulations and drug delivery systems especially in terms of liquid dosage forms [13,14]. These challenges in formulation development and drug delivery systems are a poor dissolution rate, poor oral absorption, and poor bioavailability after oral administration [14].

Over many years, the pharmaceutical industry has recognized the value of solubility expertise [15,16]. By enabling chemists/scientists to make useful decisions, the solubility data of drugs, particularly in the area of drug development and research, provides useful information to enhance the quality of drug candidates and enhance the success

rate clinically [17]. Additionally, the estimation of *in vivo* pharmacokinetics using solubility data enhances dose prediction [18,19]. The cosolvency technique, one of many that have been researched to enhance the solubility of medications [20–23], has been widely used in pharmaceutical science and practice [19]. In order to increase the solubility of ITN in this work, the cosolvency technique was applied with dimethyl sulfoxide (DMSO) [Figure 1B], as a cosolvent. The enhancement in ITN solubility using DMSO could resolve several issues of ITN, such as poor aqueous solubility, a poor dissolution rate, poor oral absorption, and poor bioavailability problems. Pharmaceutical drug solubility data are an important physicochemical attribute for a number of industrial processes, including manufacturing, formulation development, and other uses [24–26]. The solubilization of ITN in solutions of water (H₂O) and a cosolvent has not been well reported. To change the physicochemical and basic properties of ITN, a variety of lipid-based formulations, including microemulsions, microemulsion gels, and self-nanoemulsifying formulations, was investigated [27–32]. The solubility of ITN in a few environmentally friendly solvents, such as propylene glycol (PG), polyethylene glycol-400 (PEG-400), and carbitol, has been documented at room temperature [28,31]. At temperatures ranging from 298.2 to 318.2 K and an atmospheric pressure of 101.1 kPa, we previously reported the solubility and thermodynamic data of ITN in 11 distinct green solvents, namely H₂O, methanol, ethanol, 1-butanol, 2-butanol, ethylene glycol, PG, PEG-400, ethyl acetate, carbitol, and DMSO [33].

The stock solution of DMSO has been utilized as a *de facto* standard for the storage of numerous substances and the distribution of various assays, including solubility assessment [34]. In addition, DMSO is one of the most commonly used cosolvents for solubility enhancement due to its complete miscibility with H₂O and low chemical reactivity [34,35]. The main limitation of using DMSO is that it affects enzyme activity and cell growth [36]. DMSO is known to influence the protein–ligand binding via solvent viscosity effects and hence it could influence the drug kinetics of the *in vivo*'s drug disposition [35,37]. It has been reported to reduce ligand–protein binding, which could result in an improved kinetics profile of the drug disposition [35]. The solubility of several weakly soluble pharmaceutical compounds, including raloxifene hydrochloride, sinapic acid, pyridazinone derivatives, baricitinib, meloxicam, and clozapine, has been enhanced using DMSO as a potential solubilizer/cosolvent [26,38–42]. There is no information in the literature regarding the solubility data and thermodynamic parameters of ITN (3) in numerous {DMSO (1) + H₂O (2)} mixtures at different temperatures (298.2–318.2 K) under constant atmospheric pressure (101.1 kPa). Therefore, this investigation was conducted to determine the solubility and thermodynamic parameters of ITN (3) in numerous {DMSO (1) + H₂O (2)} mixes, including pure DMSO and H₂O, at 298.2–318.2 K under atmospheric pressure. The information acquired during the data collection phase of the study may be helpful for the development of dosage forms, pre-formulation studies, and purification of the studied drug.

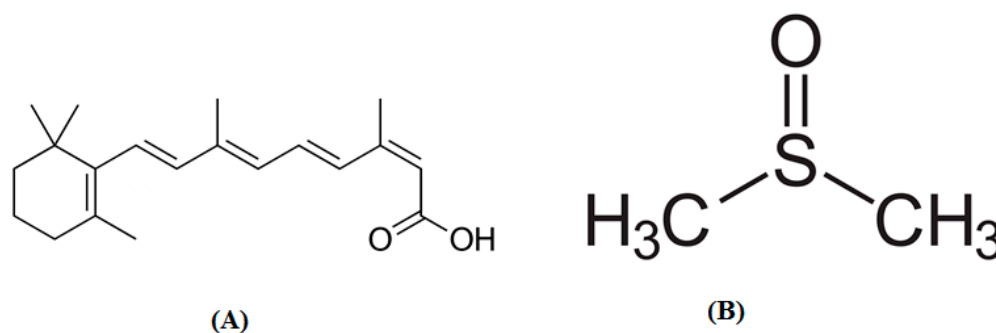


Figure 1. Molecular structures/formulae of (A) isotretinoin (ITN) and (B) dimethyl sulfoxide (DMSO).

2. Results and Discussion

2.1. Solid-State Characterization and Experimental Solubility Data of ITN

The solid-phase characterization of ITN before solubility determination (pure ITN) and after solubility determination (equilibrated ITN) was carried out to investigate the possibility of ITN evolving into polymorphs or solvates/hydrates. The findings of this characterization on pure and equilibrated ITN using differential scanning calorimetry (DSC), powder X-ray diffraction (PXRD), and Fourier transforms infrared spectroscopy (FTIR) investigations are presented in our most recent work [33]. The FTIR, DSC, and PXRD spectra of both samples of ITN were said to be similar and to exhibit similar peak characteristics in our most recent paper [33]. Furthermore, the equilibrated ITN sample did not exhibit any additional FTIR, DSC, or PXRD peaks. According to these results, ITN did not transform into polymorphs or solvates/hydrates. The experimental solubility values of ITN (3) in numerous {DMSO (1) + H₂O (2)} mixtures at five distinct temperatures and constant pressure are mentioned in Table 1.

Table 1. Experimental (x_e) and ideal solubility (x^{idl}) data of ITN (3) in binary {DMSO (1) + H₂O (2)} mixes at 298.2–318.2 K and 101.1 kPa ^a (values in parentheses are standard deviations).

m^a	x_e^b				
	$T = 298.2 \text{ K}$	$T = 303.2 \text{ K}$	$T = 308.2 \text{ K}$	$T = 313.2 \text{ K}$	$T = 318.2 \text{ K}$
0.0	$3.10 (0.07) \times 10^{-7}$	$4.60 (0.15) \times 10^{-7}$	$7.50 (0.18) \times 10^{-7}$	$1.10 (0.02) \times 10^{-6}$	$1.50 (0.03) \times 10^{-6}$
0.1	$1.12 (0.02) \times 10^{-6}$	$1.59 (0.03) \times 10^{-6}$	$2.45 (0.05) \times 10^{-6}$	$3.47 (0.06) \times 10^{-6}$	$4.61 (0.11) \times 10^{-6}$
0.2	$3.83 (0.08) \times 10^{-6}$	$5.28 (0.17) \times 10^{-6}$	$7.87 (0.21) \times 10^{-6}$	$1.10 (0.01) \times 10^{-5}$	$1.42 (0.02) \times 10^{-5}$
0.3	$1.36 (0.01) \times 10^{-5}$	$1.82 (0.03) \times 10^{-5}$	$2.57 (0.04) \times 10^{-5}$	$3.43 (0.06) \times 10^{-5}$	$4.29 (0.07) \times 10^{-5}$
0.4	$4.68 (0.07) \times 10^{-5}$	$6.06 (0.08) \times 10^{-5}$	$8.23 (0.10) \times 10^{-5}$	$1.08 (0.01) \times 10^{-4}$	$1.32 (0.02) \times 10^{-4}$
0.5	$1.65 (0.04) \times 10^{-4}$	$2.05 (0.05) \times 10^{-4}$	$2.69 (0.06) \times 10^{-4}$	$3.31 (0.07) \times 10^{-4}$	$3.96 (0.08) \times 10^{-4}$
0.6	$5.70 (0.10) \times 10^{-4}$	$6.88 (0.12) \times 10^{-4}$	$8.57 (0.17) \times 10^{-4}$	$1.08 (0.01) \times 10^{-3}$	$1.22 (0.02) \times 10^{-3}$
0.7	$2.02 (0.03) \times 10^{-3}$	$2.33 (0.05) \times 10^{-3}$	$2.79 (0.06) \times 10^{-3}$	$3.24 (0.07) \times 10^{-3}$	$3.66 (0.08) \times 10^{-3}$
0.8	$6.97 (0.10) \times 10^{-3}$	$7.81 (0.12) \times 10^{-3}$	$8.96 (0.20) \times 10^{-3}$	$1.02 (0.01) \times 10^{-2}$	$1.15 (0.01) \times 10^{-2}$
0.9	$2.44 (0.02) \times 10^{-2}$	$2.66 (0.03) \times 10^{-2}$	$2.86 (0.03) \times 10^{-2}$	$3.19 (0.04) \times 10^{-2}$	$3.39 (0.05) \times 10^{-2}$
1.0	$8.47 (0.10) \times 10^{-2}$	$8.88 (0.11) \times 10^{-2}$	$9.31 (0.12) \times 10^{-2}$	$9.80 (0.13) \times 10^{-2}$	$1.02 (0.01) \times 10^{-1}$
x^{idl}	$4.28 (0.03) \times 10^{-2}$	$4.43 (0.04) \times 10^{-2}$	$4.58 (0.05) \times 10^{-2}$	$4.73 (0.06) \times 10^{-2}$	$4.88 (0.07) \times 10^{-2}$

^a The uncertainties u are $u(T) = 0.18 \text{ K}$, $u(m) = 0.0007$, and $u(p) = 2 \text{ kPa}$. ^b The relative uncertainty u_r in solubility is $u_r(x_e) = 0.04$.

ITN solubility (3) in numerous {DMSO (1) + H₂O (2)} mixes has not been documented. At 298.2–318.2 K, ITN mole fraction solubility data in pure DMSO and H₂O have been recorded [33]. Figure 2 compares graphically the experimental and literature solubility data of ITN in pure H₂O and DMSO at 298.2–318.2 K. According to the findings shown in Figure 2, there was a strong correlation between the experimental solubility data of ITN in pure H₂O and DMSO and those mentioned in the literature [33]. These findings showed that ITN's experimental solubility statistics agreed well with previously published research [33]. In general, it was found that neat DMSO and neat H₂O had the highest and lowest mole fraction solubilities of ITN, respectively. The low polarity of DMSO in contrast to the high polarity of H₂O may be the cause of ITN's greatest solubility in pure DMSO [38–40]. In addition, the enhanced ITN solubility in DMSO could be due to intermolecular interactions between –COOH groups of ITN (Figure 1A) with S=O groups of DMSO (Figure 1B). Temperature and the mass fraction of DMSO both increased the mole fraction solubility of ITN (3) in different {DMSO (1) + H₂O (2)} solutions. The effect of the DMSO mass fraction on the solubility of ITN in logarithmic mole fractions was also investigated between 298.2 and 318.2 K. Figure 3 provides documentation on the outcomes. At each temperature under study, the ITN solubility increased linearly with the DMSO mass fraction in mixes of {DMSO (1) + H₂O (2)}. The solubility of ITN in mole fractions increased significantly from neat H₂O to neat DMSO. Solubilizing ITN in an aqueous media could potentially use DMSO as a solubilizer or cosolvent.

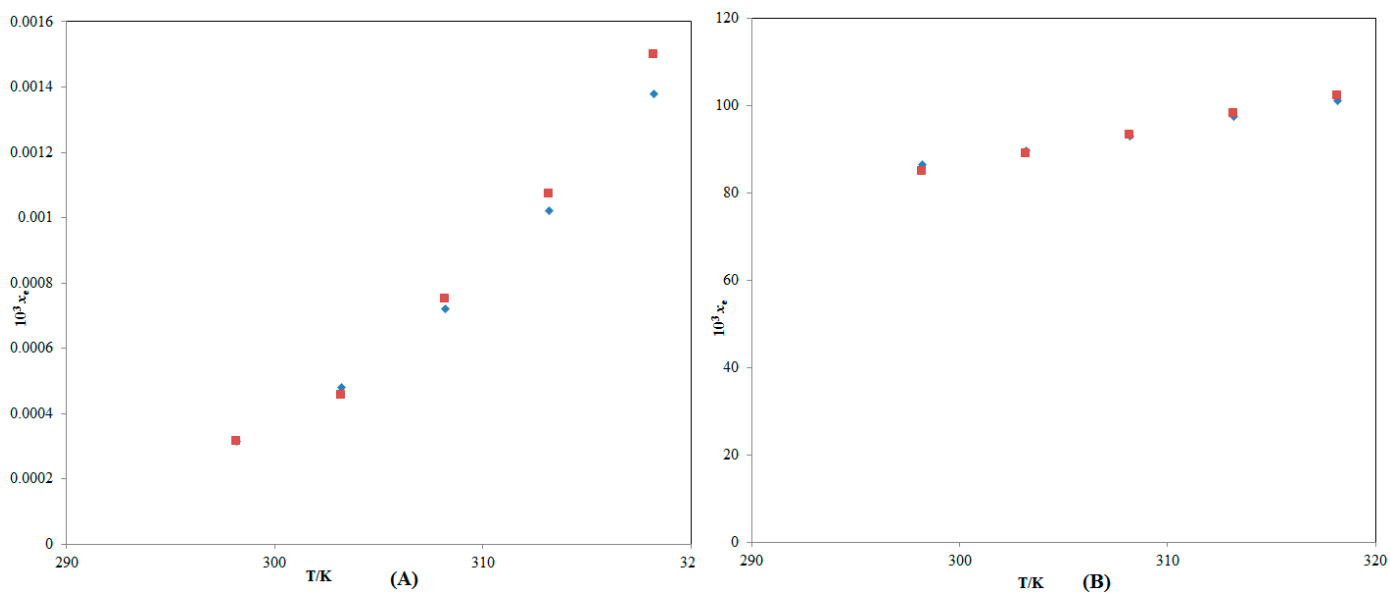


Figure 2. Graphic comparison between ITN mole fraction solubility data (x_e) in (A) pure H₂O and (B) pure DMSO with those found in the literature at 298.2–318.2 K. The symbol \blacksquare indicates the stated mole fraction solubilities of ITN in (A) pure H₂O and (B) pure DMSO, and the symbol \blacklozenge indicates the literature solubilities of ITN in (A) pure H₂O and (B) pure DMSO retrieved from reference [33].

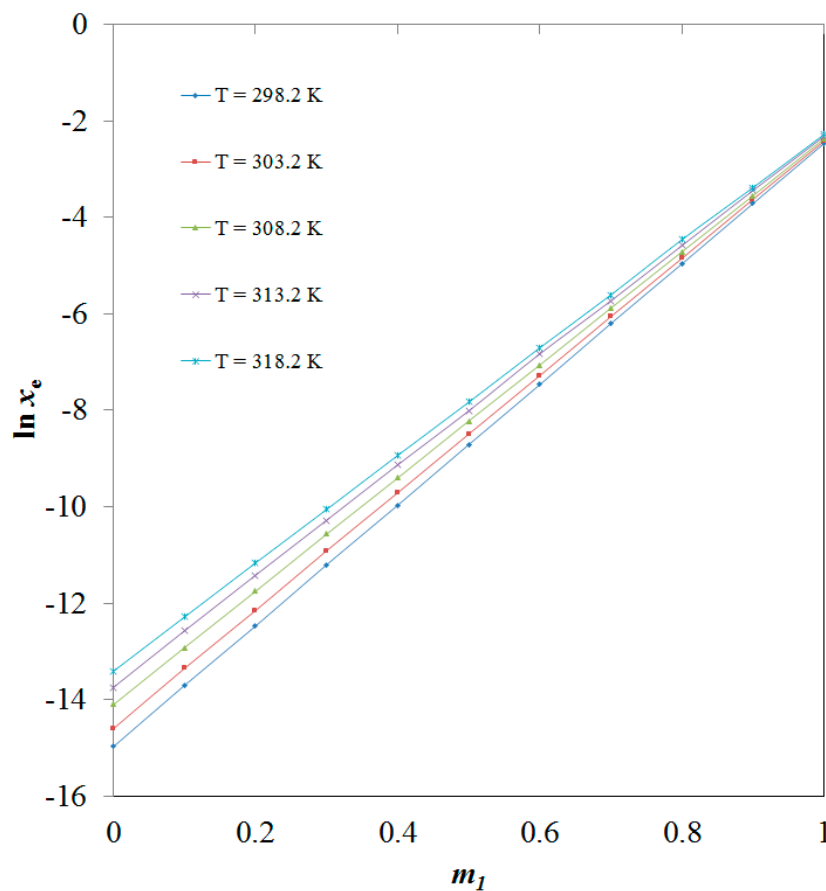


Figure 3. Effect of DMSO mass fraction (m_1) on ITN solubility values (x_e) at 298.2–318.2 K.

2.2. Determination of Hansen Solubility Parameters (HSPs)

ITN's total HSP (δ_t) was derived using reference [33], and it was found to be 19.30 MPa^{1/2}, suggesting low polarity. The HSP values for neat DMSO (δ_1) and neat H₂O (δ_2) are 23.60 MPa^{1/2} and 47.80 MPa^{1/2}, respectively, according to the literature [33]. Calculations revealed that the range of HSP for different {DMSO (1) + H₂O (2)} mixtures free of ITN (δ_{mix}) was between 26.02 and 45.38 MPa^{1/2}. It was found that the δ_{mix} values fell in {DMSO (1) + H₂O (2)} combinations as the DMSO mass percentage increased. As a result, DMSO mass fraction (m) = 0.1 and m = 0.9, respectively, were used to obtain the maximum and minimum δ_{mix} values. It was discovered, however, that a reduction in δ_{mix} values enhanced the solubility values of ITN. ITN (δ_t = 19.30 MPa^{1/2}) and pure DMSO (δ_1 = 23.60 MPa^{1/2}) had HSPs that were generally close to one another. The examinations further revealed the greatest solubility of ITN in neat DMSO. Because of this, the ITN solubility data from experiments employing {DMSO (1) + H₂O (2)} mixes closely mirrored these findings.

2.3. Ideal Solubility and Molecular Interactions

Table 1 displays the ideal solubility (x^{idl}) values for ITN. The calculated values for ITN's x^{idl} range from 4.28×10^{-2} to 4.88×10^{-2} at 298.2–318.2 K. ITN exhibited substantially higher x^{idl} values than experimental solubility (x_e) values in pure H₂O. At all temperatures examined, ITN's x_e values were higher than its x^{idl} values in pure DMSO. Because ITN is most soluble in pure DMSO, it can be used as the best cosolvent for ITN solubilization.

Table 2 displays the activity coefficient (γ_i) values for ITN in various {DMSO (1) + H₂O (2)} combinations at 298.2–318.2 K. At each of the studied temperatures, the ITN's γ_i value was at its highest in pure H₂O. But at each temperature considered, the γ_i of ITN was lowest in pure DMSO. In comparison to neat H₂O, the γ_i values for ITN were substantially lower for neat DMSO. The highest γ_i for ITN in neat H₂O may be explained by the least solubility of ITN in H₂O. These outcomes suggest that, when compared to the ITN–H₂O combination, the ITN–DMSO combination has the greatest number of solute–solvent interactions at the molecular level.

Table 2. Activity coefficients (γ_i) of ITN in numerous {DMSO (1) + H₂O (2)} combinations at 298.2–318.2 K.

m	γ_i				
	$T = 298.2 \text{ K}$	$T = 303.2 \text{ K}$	$T = 308.2 \text{ K}$	$T = 313.2 \text{ K}$	$T = 318.2 \text{ K}$
0.0	1,366,467	972,627.0	611,320.0	441,076.0	326,128.0
0.1	384,000.0	278,000.0	187,000.0	136,000.0	106,000.0
0.2	111,979.0	83,952.80	58,249.00	43,099.10	34,943.20
0.3	31,441.80	24,298.30	17,811.50	13,802.30	11,402.70
0.4	9161.740	7310.360	5568.540	4372.740	3713.1570
0.5	2602.340	2166.250	1703.980	1429.250	1233.060
0.6	751.8650	644.3650	534.7140	438.6560	399.5110
0.7	211.8050	189.9250	164.4500	146.1890	133.4190
0.8	61.48640	56.71900	51.11100	46.46460	42.45130
0.9	17.59830	16.68020	16.02050	14.83990	14.41810
1.0	5.057310	4.988350	4.918850	4.828590	4.790800

2.4. Correlation of ITN Solubility Data

ITN's solubility values were correlated by six different computational models, like "van't Hoff, Apelblat, Buchowski-Ksiazczak λh , Yalkowsky-Roseman, Jouyban-Acree, and Jouyban-Acree-van't Hoff models" [26,43–51]. Table 3 displays the findings concerning the correlation with the "van't Hoff model". It was determined that this model's overall root mean square deviation (RMSD) was 1.87%. For all cosolvent mixtures as well as neat DMSO and H₂O, the determination coefficient (R^2) for ITN was calculated to be 0.9940 to

0.9992. Results from the “van’t Hoff model” and ITN (3) experimental solubility values in mixes of {DMSO (1) + H₂O (2)} showed a strong correlation.

Table 3. Outcomes for the “van’t Hoff model” in terms of model parameters (*a* and *b*), *R*², and *RMSD* for ITN (3) in numerous {DMSO (1) + H₂O (2)} mixtures (values in parentheses are standard deviations of model parameters).

<i>m</i>	<i>a</i>	<i>b</i>	<i>R</i> ²	Overall <i>RMSD</i> (%)
0.0	10.402 (0.34)	−7568.3 (512.12)	0.9966	
0.1	9.3196 (0.32)	−6865.0 (432.41)	0.9971	
0.2	8.8695 (0.30)	−6364.6 (402.15)	0.9967	
0.3	7.4104 (0.27)	−5549.1 (321.27)	0.9969	
0.4	6.9041 (0.22)	−5031.7 (301.43)	0.9968	
0.5	5.5507 (0.17)	−4252.5 (284.81)	0.9967	1.87
0.6	5.1279 (0.16)	−3757.5 (253.58)	0.9940	
0.7	3.4432 (0.10)	−2877.3 (194.29)	0.9978	
0.8	3.1037 (0.09)	−2408.9 (180.21)	0.9988	
0.9	1.6606 (0.05)	−1603.6 (64.29)	0.9948	
1.0	0.52410 (0.01)	−892.54 (28.41)	0.9992	

In binary solvent mixes, pure H₂O, and DMSO, experimental and Apelblat solubility data for ITN are graphically correlated in Figure 4. The findings shown in Figure 4 reveal that the experimental solubility values of ITN and the “Apelblat model” correlated well. In Table 4, the Apelblat model parameters and correlation findings for ITN in binary {DMSO (1) + H₂O (2)} mixes are shown. It was determined that this model’s overall *RMSD* was 1.69%. Including pure DMSO and H₂O, ITN (3) demonstrated an *R*² of 0.9951–0.9994 in all cosolvent combinations. A significant correlation was also found between the results of the “Apelblat model” and the experimental ITN (3) solubility values in numerous {DMSO (1) + H₂O (2)} mixes.

Table 4. Outcomes of the “Apelblat model” in terms of model parameters (*A*, *B*, and *C*), *R*², and *RMSD* for ITN (3) in numerous {DMSO (1) + H₂O (2)} mixes (values in parentheses are standard deviations of model coefficients).

<i>m</i>	<i>A</i>	<i>B</i>	<i>C</i>	<i>R</i> ²	Overall <i>RMSD</i> (%)
0.0	454.09 (31.12)	−27954 (182.26)	−65.877 (6.71)	0.9969	
0.1	563.01 (34.58)	−32298 (203.31)	−82.214 (8.45)	0.9978	
0.2	512.95 (32.81)	−29519 (188.16)	−74.847 (7.71)	0.9974	
0.3	521.99 (33.10)	−29183 (183.24)	−76.408 (7.93)	0.9979	
0.4	436.22 (29.82)	−24751 (174.34)	−63.746 (6.94)	0.9977	
0.5	344.90 (26.24)	−19840 (121.63)	−50.388 (5.13)	0.9974	1.69
0.6	347.63 (26.31)	−19489 (119.06)	−50.857 (5.16)	0.9951	
0.7	126.23 (6.13)	−8521.8 (64.31)	−18.230 (1.57)	0.9980	
0.8	−148.36 (7.21)	4553.4 (44.12)	22.479 (1.77)	0.9994	
0.9	44.494 (2.84)	−3574.5 (38.84)	−6.3581 (0.76)	0.9950	
1.0	11.915 (1.01)	−1418.1 (22.89)	−1.6901 (0.10)	0.9992	

The findings of the “Buchowski-Ksiazaczak *λh*” correlation for ITN in cosolvent mixtures and neat solvents are shown in Table 5. It was determined that this model’s overall *RMSD* was 3.15%. These results also show a strong agreement between the experimental solubility values from ITN and the “Buchowski-Ksiazaczak *λh* model”.

The results of the correlation with the “Yalkowsky-Roseman model” are shown in Table 6. It was determined that this model’s overall *RMSD* was 2.10%, suggesting a satisfactory connection between the “Yalkowsky-Roseman model” and the solubility data for ITN (3) in various {DMSO (1) + H₂O (2)} combinations.

Table 5. Outcomes of “Buchowski-Ksiazaczak λh model” for ITN (3) in numerous {DMSO (1) + H₂O (2)} mixes (values in parentheses are standard deviations of model parameters).

m	λ	h	Overall RMSD (%)
0.0	5.3156 (0.86)	1423.8 (31.23)	3.15
0.1	4.8451 (0.83)	1416.9 (30.62)	
0.2	4.1898 (0.75)	1519.0 (33.18)	
0.3	3.8473 (0.66)	1442.3 (32.51)	
0.4	3.2108 (0.51)	1567.0 (34.21)	
0.5	2.8430 (0.42)	1495.8 (32.91)	
0.6	2.1723 (0.27)	1729.7 (38.44)	
0.7	1.9127 (0.12)	1504.3 (33.61)	
0.8	1.2176 (0.10)	1978.4 (41.18)	
0.9	0.88170 (0.01)	1818.7 (39.42)	
1.0	0.44750 (0.02)	1994.4 (42.12)	

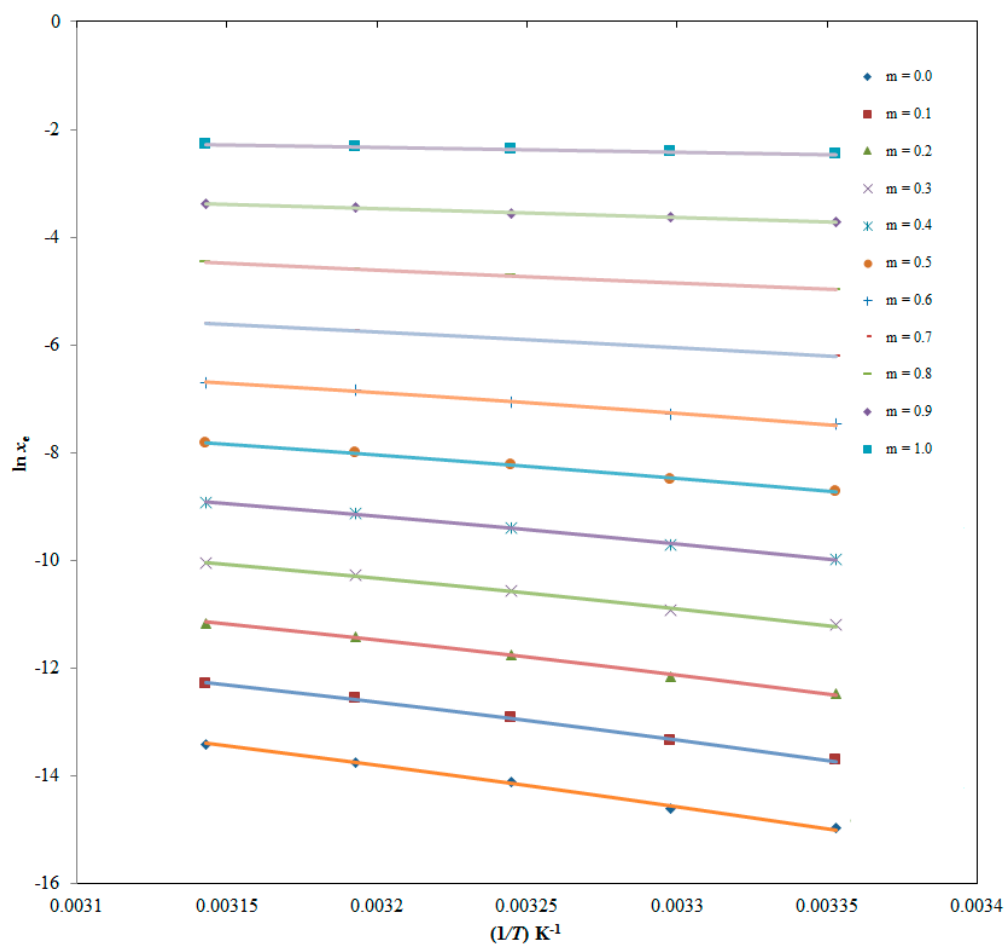
**Figure 4.** Graphical comparison of experimental ITN (3) solubility data (x_e) with “Apelblat model” in numerous {DMSO (1) + H₂O (2)} mixes (DMSO mass fraction $m = 0.0$ – 1.0) against $1/T$; symbols indicate the experimental ITN solubility data, whereas solid lines indicate the “Apelblat model” ITN solubility data.

Table 6. Findings of “Yalkowsky-Roseman model” for ITN (3) in several {DMSO (1) + H₂O (2)} combinations at 298.2–318.2 K.

<i>m</i>	$\log x^{\text{Yal}}$					Overall RMSD (%)
	<i>T</i> = 298.2 K	<i>T</i> = 303.2 K	<i>T</i> = 308.2 K	<i>T</i> = 313.2 K	<i>T</i> = 318.2 K	
0.1	−5.96	−5.80	−5.61	−5.46	−5.34	2.10
0.2	−5.42	−5.28	−5.10	−4.96	−4.85	
0.3	−4.87	−4.75	−4.59	−4.47	−4.37	
0.4	−4.33	−4.22	−4.08	−3.97	−3.89	
0.5	−3.79	−3.69	−3.57	−3.48	−3.40	
0.6	−3.24	−3.16	−3.06	−2.98	−2.92	
0.7	−2.70	−2.63	−2.55	−2.49	−2.44	
0.8	−2.15	−2.10	−2.04	−1.99	−1.95	
0.9	−1.61	−1.57	−1.54	−1.50	−1.47	

In several {DMSO (1) + H₂O (2)} mixes at varied temperatures and in varied solvent mixes, the solubility value of ITN (3) was likewise correlated to “Jouyban-Acree and Jouyban-Acree-van’t Hoff models” [51]. The results of the correlation with the “Jouyban-Acree and Jouyban-Acree-van’t Hoff models” are shown in Table 7. According to the calculations, the overall RMSDs for the “Jouyban-Acree and Jouyban-Acree-van’t Hoff models” are 1.02% and 1.15%, respectively.

Table 7. Findings of “Jouyban-Acree” and “Jouyban-Acree-van’t Hoff” models for ITN (3) in different {DMSO (1) + H₂O (2)} mixtures (values in parentheses are standard deviations of model parameters).

System	Jouyban-Acree	Jouyban-Acree-van’t Hoff
{DMSO (1) + H ₂ O (2)}	<i>J_i</i> 30,624 (561.32)	<i>A</i> ₁ 0.52410 (0.01) <i>B</i> ₁ −892.54 (28.41) <i>A</i> ₂ 10.402 (0.34) <i>B</i> ₂ −7568.3 (512.12)
RMSD (%)	1.02	<i>J_i</i> 29,178 (532.41) 1.15

2.5. Thermodynamic Parameters for ITN Dissolution

The van’t Hoff method was used to derive apparent standard enthalpy ($\Delta_{\text{sol}}H^\circ$) values for ITN in all cosolvent mixtures as well as neat DMSO and H₂O. The linear van’t Hoff graphs of ITN in all cosolvent mixtures, as well as in pure DMSO and H₂O, are shown in Figure 5 where $R^2 > 0.99$ was determined, as shown in Table 8. The results for all thermodynamic parameters are likewise shown in Table 8. ITN (3) $\Delta_{\text{sol}}H^\circ$ values in numerous {DMSO (1) + H₂O (2)} mixes and neat DMSO and H₂O ranged from 7.430 to 63.00 kJ mol^{−1}. ITN (3) apparent standard Gibbs energy ($\Delta_{\text{sol}}G^\circ$) values in various {DMSO (1) + H₂O (2)} mixes and neat DMSO and H₂O ranged from 6.077 to 36.27 kJ mol^{−1}. These results for ITN’s $\Delta_{\text{sol}}H^\circ$ and $\Delta_{\text{sol}}G^\circ$ revealed “endothermic dissolution” of ITN (3) in various {DMSO (1) + H₂O (2)} mixes as well as neat DMSO and H₂O [26,38]. ITN (3) apparent standard entropy ($\Delta_{\text{sol}}S^\circ$) values between 4.392 and 86.78 J mol^{−1} K^{−1} were obtained in numerous {DMSO (1) + H₂O (2)} mixes as well as in neat DMSO and H₂O, showing that entropy-driven ITN (3) dissolution occurs in these binary mixtures [26]. In all {DMSO (1) + H₂O (2)} mixes, including neat DMSO and H₂O, it was discovered that the dissolution of ITN (3) was “endothermic and entropy-driven” [26,38].

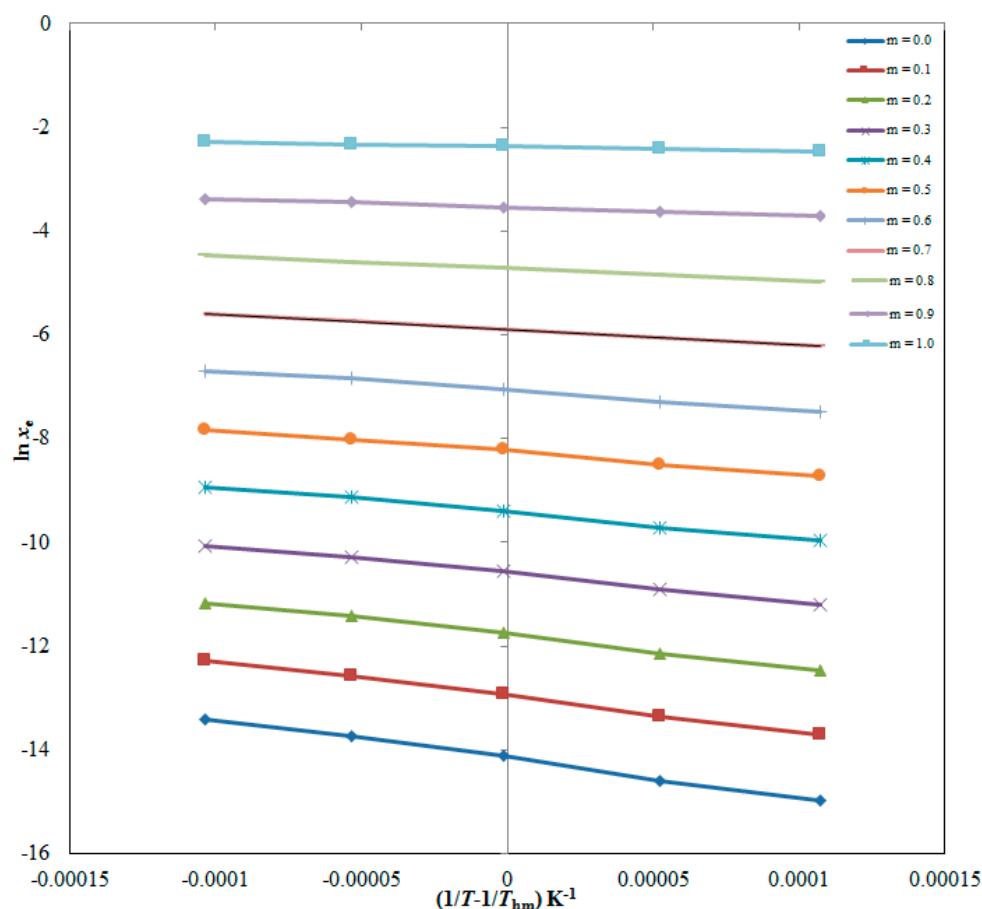


Figure 5. van't Hoff plots at the mean harmonic temperature (T_{hm}) for ITN created between logarithmic mole fraction solubility ($\ln x_e$) and $1/T - 1/T_{hm}$ for ITN in numerous {DMSO (1) + H₂O (2)} mixtures (DMSO mass fraction $m = 0.0$ – 1.0).

Table 8. Apparent thermodynamic parameters ($\Delta_{sol}H^0$, $\Delta_{sol}G^0$, and $\Delta_{sol}S^0$) along with R^2 values for ITN (3) in different {DMSO (1) + H₂O (2)} mixtures ^c (values in parentheses are standard deviations of thermodynamic parameters).

m	$\Delta_{sol}H^0/\text{kJ mol}^{-1}$	$\Delta_{sol}G^0/\text{kJ mol}^{-1}$	$\Delta_{sol}S^0/\text{J mol}^{-1} \text{K}^{-1}$	R^2
0.0	63.00 (0.76)	36.27 (0.43)	86.78 (1.12)	0.9966
0.1	57.15 (0.67)	33.20 (0.41)	77.75 (1.03)	0.9971
0.2	52.98 (0.63)	30.19 (0.39)	73.99 (1.00)	0.9967
0.3	46.19 (0.52)	27.15 (0.37)	61.83 (0.98)	0.9969
0.4	41.89 (0.48)	24.14 (0.36)	57.59 (0.92)	0.9968
0.5	35.40 (0.42)	21.13 (0.30)	46.31 (0.81)	0.9967
0.6	31.28 (0.40)	18.10 (0.26)	42.78 (0.74)	0.9940
0.7	23.95 (0.32)	15.10 (0.24)	28.74 (0.56)	0.9978
0.8	20.05 (0.28)	12.07 (0.20)	25.90 (0.48)	0.9989
0.9	13.35 (0.22)	9.078 (0.14)	13.87 (0.23)	0.9948
1.0	7.430 (0.10)	6.077 (0.09)	4.392 (0.10)	0.9992

^c The relative uncertainties are $u(\Delta_{sol}H^0) = 0.051$, $u(\Delta_{sol}G^0) = 0.047$ and $u(\Delta_{sol}S^0) = 0.057$.

2.6. Enthalpy–Entropy Compensation Analysis

An enthalpy–entropy compensation analysis was utilized to study the solvation behavior of ITN (3) in various {DMSO (1) + H₂O (2)} mixes as well as pure DMSO and H₂O. The results are presented in Figure 6. Figure 6 demonstrates that ITN (3) delivers a linear $\Delta_{sol}H^0$ vs. $\Delta_{sol}G^0$ curve in all {DMSO (1) + H₂O (2)} mixtures with neat DMSO and H₂O, with a slope of larger than 1.0 and R^2 of greater than 0.99. Based on these findings, it is predicted

that the ITN (3) solvation driven mechanism is enthalpy-driven in all {DMSO (1) + H₂O (2)} mixes as well as in neat DMSO and H₂O. The fact that ITN solvates more effectively in pure DMSO molecules than in neat H₂O molecules should be used to explain this mechanism of ITN solvation [26,38]. This led to stronger interactions between ITN-DMSO molecules than ITN-H₂O molecules. ITN (3) solvated similarly to raloxifene hydrochloride, sinapic acid, pyridazinone derivatives, and baricitinib in numerous {DMSO (1) + H₂O (2)} mixes as well as in neat DMSO and H₂O [26,38–40].

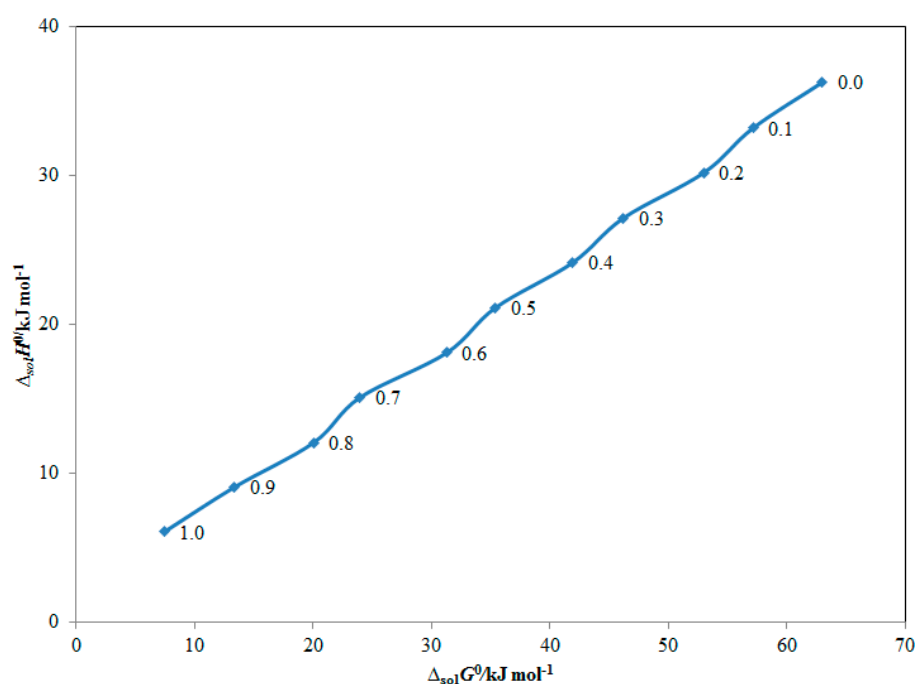


Figure 6. Apparent standard enthalpy ($\Delta_{\text{sol}}H^\circ$) vs. apparent standard Gibbs energy ($\Delta_{\text{sol}}G^\circ$) enthalpy-entropy compensation analysis for solubility of ITN in various {DMSO (1) + H₂O (2)} mixtures at the mean harmonic temperature (T_{hm}) = 308 K (DMSO mass fraction $m = 0.0$ – 1.0).

3. Materials and Methods

3.1. Materials

ITN was acquired from BOC Sciences (Shirley, NY, USA). DMSO was procured from Sigma Aldrich (St. Louis, MO, USA). Purified H₂O was procured via a Milli-Q device. The details of each material are summarized in Table 9.

Table 9. Summary of materials used.

Material	Molecular Formula	Molar Mass (g mol ⁻¹)	CAS RN	Purification Method	Mass Fraction Purity	Analysis Method	Source
ITN	C ₂₀ H ₂₈ O ₂	300.40	4759-48-2	None	>0.98	HPLC	BOC Sciences
DMSO	C ₂ H ₆ OS	78.13	67-68-5	None	>0.99	GC	Sigma Aldrich
Water	H ₂ O	18.07	7732-18-5	None	-	-	Milli-Q

ITN: isotretinoin; DMSO: dimethyl sulfoxide; HPLC: high-performance liquid chromatography; GC: gas chromatography.

3.2. Determination of ITN (3) Solubility in {DMSO (1) + H₂O (2)} Mixes

Mass measurements of all {DMSO (1) + H₂O (2)} combinations were taken by a digital analytical balance (Mettler Toledo, Greifensee, Switzerland), which had a sensitivity of 0.10 mg. A series of {DMSO (1) + H₂O (2)} solutions, with DMSO mass percentages ranging from 0.10 to 0.90, was examined. Three replicates of each {DMSO (1) + H₂O (2)} combination were taken [26]. ITN's mole fraction solubility versus mass fraction of DMSO

($m = 0.0$ – 1.0) and neat DMSO and H₂O was measured using a shake flask approach at 298.2–318.2 K and 101.1 kPa [52]. In essence, the known amounts of each {DMSO (1) + H₂O (2)} combination and neat DMSO and H₂O were combined with extra ITN crystals in triplicate. The equilibrium was achieved by saturating the resultant mixes in a WiseBath[®] WSB shaking water bath (Model WSB-18/30/-45, Daihan Scientific Co. Ltd., Seoul, Korea) at a shaking speed of 100 rpm for 72 h [33]. In order to evaluate the equilibrium time, the preliminary experiments were performed at different time intervals. It was found that there was negligible change in solubility after 72 h and hence it was selected as the equilibrium time. The saturated solutions were again removed from the shaker after they had reached equilibrium and centrifuged for 30 min at 5000 rpm. A previously established environmentally friendly HPLC method was used to assess the ITN content after the supernatants were isolated and diluted (as required) [53]. The identification of ITN was carried out via a Nucleodur (dimensions: 150 mm × 4.6 mm and particle size: 5 μm) reversed-phase C₁₈ analytical column at 298.2 K. The environmentally friendly mobile used was a binary mixture of ethyl acetate and ethanol (50:50% v v⁻¹). The mobile phase was delivered with a flow speed of 1 mL min⁻¹. The ITN measurements were performed at a wavelength of 354 nm. The sample volume was 20 μL, which was injected using a Waters autosampler. The Analytical GREENess (AGREE) score was determined to evaluate the eco-friendliness nature of the HPLC method. The AGREE score was predicted to be 0.76 for the present HPLC method, indicating the eco-friendly nature of the HPLC method [53]. ITN mole fraction solubilities (x_e) were calculated using their standard formulae described in our previous work [38–40].

3.3. HSPs of ITN and Numerous {DMSO (1) + H₂O (2)} Combinations

A drug's HSP is directly correlated with how well it dissolves in a neat solvent or cosolvent–H₂O combination. A medication will reportedly have the highest solubility in a certain solvent when its HSP is close to that solvent's [54]. As a result, the HSPs for the research medication ITN, neat DMSO, and neat H₂O were calculated. ITN, neat H₂O, and neat DMSO δ_t values were derived from reference [33].

Using Equation (1), the δ_{mix} was calculated [55]:

$$\delta_{\text{mix}} = \alpha \delta_1 + (1 - \alpha) \delta_2 \quad (1)$$

where α is the DMSO volume percentage in the mixture of {DMSO (1) + H₂O (2)}.

3.4. ITN Ideal Solubility and Molecular Interactions

Using Equation (2), we derived the x^{idl} of ITN at 298.2–318.2 K [56]:

$$\ln x^{\text{idl}} = \frac{-\Delta H_{\text{fus}}(T_{\text{fus}} - T)}{RT_{\text{fus}}T} + \left(\frac{\Delta C_p}{R}\right) \left[\frac{T_{\text{fus}} - T}{T} + \ln\left(\frac{T}{T_{\text{fus}}}\right)\right] \quad (2)$$

where T is an absolute temperature; T_{fus} is the ITN fusion/melting temperature; R is a universal gas constant; ΔH_{fus} is the ITN fusion enthalpy, and ΔC_p is the difference in the molar heat capacity of the ITN solid state with its liquid state [57]. Equation (3) was utilized to derive the ΔC_p for ITN [56,57]:

$$\Delta C_p = \frac{\Delta H_{\text{fus}}}{T_{\text{fus}}} \quad (3)$$

The T_{fus} and ΔH_{fus} values for ITN were taken as 452.7 K and 7.64 kJ mol⁻¹, respectively from reference [33]. The ΔC_p for ITN was calculated to be 16.67 J mol⁻¹ K⁻¹ using Equation (3). Finally, the x^{idl} values for ITN were derived from Equation (2). Equation (4) was used to derive the γ_i values for ITN in numerous {DMSO (1) + H₂O (2)} mixes including neat DMSO and H₂O [56,58]:

$$\gamma_i = \frac{x^{\text{idl}}}{x_e} \quad (4)$$

The chemical basis of molecular interactions between the solute and solvent was explained using ITN γ_1 values.

3.5. Correlation of ITN Solubility with Computational Models

The computational verification of experimental drug solubility data is crucial for practical predictions and validations [43,44]. For the correlation of the experimental solubility data of ITN, six distinct computational models, namely “van’t Hoff, Apelblat, Buchowski-Ksiazczak λh , Yalkowsky-Roseman, Jouyban-Acree, and Jouyban-Acree-van’t Hoff models”, were utilized [26,43–51]. The program used for all modeling tasks was MS Excel 2013. “van’t Hoff model solubility ($x^{\text{van't}}$)” of ITN (3) in binary {DMSO (1) + H₂O (2)} mixtures was derived via Equation (5) [26]:

$$\ln x^{\text{van't}} = a + \frac{b}{T} \quad (5)$$

where a and b are Equation (5) model parameters recorded using the least squares methodology [49]. *RMSD* was used to correlate the values x_e and $x^{\text{van't}}$ for the ITN. A formula taken from the literature was used to calculate the *RMSD* [59]. With the help of Equation (6), the “Apelblat model solubility (x^{ApI})” of ITN (3) in numerous {DMSO (1) + H₂O (2)} mixtures was derived [45,46]:

$$\ln x^{\text{ApI}} = A + \frac{B}{T} + C \ln(T) \quad (6)$$

where “nonlinear multivariate regression analysis” [59] was used to obtain the Equation (6) model parameters from the experimental ITN solubility values provided in Table 1. In terms of *RMSD*, the results from ITN’s x_e and x^{ApI} were likewise correlated. By Equation (7), the “Buchowski-Ksiazczak λh solubility ($x^{\lambda h}$)” of ITN (3) in numerous {DMSO (1) + H₂O (2)} mixtures was derived [47,48]:

$$\ln \left[1 + \frac{\lambda(1 - x^{\lambda h})}{x^{\lambda h}} \right] = \lambda h \left[\frac{1}{T} - \frac{1}{T_{\text{fus}}} \right] \quad (7)$$

where λ and h are Equation (7) model parameters.

Because Equations (5)–(7) reflect solubility data at varied temperatures in a certain solvent composition, they cannot be used to forecast the solubility data of a binary solvent combination at varied solvent compositions [51,60,61]. In order to make such forecasts, cosolvency models such as the Yalkowsky–Roseman, Jouyban–Acree, and Jouyban–Acree–van’t Hoff models are needed. With the help of Equation (8), “logarithmic solubility of Yalkowsky-Roseman model ($\log x^{\text{Yal}}$)” for ITN (3) in numerous {DMSO (1) + H₂O (2)} mixtures was derived [50]:

$$\log x^{\text{Yal}} = w_1 \log x_1 + w_2 \log x_2 \quad (8)$$

where, x_1 = ITN solubility (3) in DMSO (1); x_2 = ITN solubility in H₂O (2); w_1 = DMSO mass fraction, and w_2 = H₂O mass fraction. Drug solubility data in various solvent compositions at a given temperature are linked by Equation (8).

Equation (9) was utilized to derive the solubility of drugs in distinct cosolvent mixtures and temperature ($x_{m,T}$) via the “Jouyban-Acree model” [51]:

$$\ln x_{m,T} = w_1 \ln x_{1,T} + w_2 \ln x_{2,T} + \left(\frac{w_1 \cdot w_2}{T} \right) \sum_{i=0}^2 J_i (w_1 - w_2)^i \quad (9)$$

where $x_{1,T}$ and $x_{2,T}$ are the solubility of ITN in DMSO (1) and H₂O (2) at temperature T and J terms are Equation (9) model parameters. To calculate the solubility of ITN in cosolvent compositions at the target temperature, the solubility of ITN in neat DMSO and H₂O must

be used as input data. Equations (5) and (9) can be used to create the “Jouyban-Acree-van’t Hoff model” [51] to get around this restriction.

3.6. Thermodynamic Parameters

At the mean harmonic temperature (T_{hm}), all apparent thermodynamic parameters for ITN were determined [56]. The T_{hm} was determined using the reported equation [51,56]. The calculated T_{hm} for ITN is 308 K. An apparent thermodynamic analysis was applied to derive several thermodynamic parameters. The “van’t Hoff and Gibbs equations” were used to calculate these parameters. The $\Delta_{\text{sol}}H^0$ values for ITN (3) in various {DMSO (1) + H₂O (2)} mixtures were calculated using Equation (10) and $T_{\text{hm}} = 308$ K [47,62]:

$$\left(\frac{\partial \ln x_e}{\partial (1/T - 1/T_{\text{hm}})} \right)_P = -\frac{\Delta_{\text{sol}}H^0}{R} \quad (10)$$

The “ $\Delta_{\text{sol}}H^0$ ” for ITN was derived using the graphed “van’t Hoff” plots between the $\ln x_e$ values of ITN and $1/T - 1/T_{\text{hm}}$. The van’t Hoff plots for ITN (3) in binary {DMSO (1) + H₂O (2)} mixes are shown in Figure 5.

Additionally, at $T_{\text{hm}} = 308$ K, the $\Delta_{\text{sol}}G^0$ for ITN (3) in binary {DMSO (1) + H₂O (2)} mixes was calculated using the Krug et al. methodology via Equation (11) [62]:

$$\Delta_{\text{sol}}G^0 = -RT_{\text{hm}} \times \text{intercept} \quad (11)$$

where, the “van’t Hoff plots” shown in Figure 5 were used to determine the intercept values for ITN (3) in binary mixtures of DMSO (1) and H₂O (2).

By Equation (12), the $\Delta_{\text{sol}}S^0$ for ITN (3) in numerous {DMSO (1) + H₂O (2)} mixtures was derived [56,62,63]:

$$\Delta_{\text{sol}}S^0 = \frac{\Delta_{\text{sol}}H^0 - \Delta_{\text{sol}}G^0}{T_{\text{hm}}} \quad (12)$$

3.7. Enthalpy–Entropy Compensation Analysis

An enthalpy–entropy compensation analysis was used, as previously described [26], to evaluate the solvation behavior of ITN (3) in numerous mixes of {DMSO (1) + H₂O (2)}. Weighted curves of $\Delta_{\text{sol}}H^\circ$ vs. $\Delta_{\text{sol}}G^\circ$ were generated at $T_{\text{hm}} = 308$ K for this experiment [64,65].

4. Conclusions

The solubility of ITN in several {DMSO (1) + H₂O (2)} combinations has not yet been published. This study evaluated the solubility of ITN (3) in binary {DMSO (1) + H₂O (2)} combinations as well as neat DMSO and H₂O at various temperatures under constant pressure. In all {DMSO (1) + H₂O (2)} mixes, including neat DMSO and H₂O, ITN (3) mole fraction solubilities rose with the temperature and DMSO mass fraction. The maximum and minimum solubilities of ITN in neat DMSO and neat H₂O, respectively, were found for each temperature studied. Six distinct computational models and experimentally determined ITN (3) solubility data were highly correlated for all {DMSO (1) + H₂O (2)} mixes, including neat DMSO and H₂O. It was discovered that all thermodynamic values, including $\Delta_{\text{sol}}H^\circ$, $\Delta_{\text{sol}}G^\circ$, and $\Delta_{\text{sol}}S^\circ$, in numerous {DMSO (1) + H₂O (2)} mixes as well as pure DMSO and H₂O were positive, showing “endothermic and entropy-driven” ITN dissolution. Enthalpy drove the ITN solvation process in all {DMSO (1) + H₂O (2)} combinations as well as in pure DMSO and H₂O. The collected information from this study may be beneficial for recrystallization, purification, pre-formulation studies, and for the creation of dosage forms for the medicine under study.

Author Contributions: Conceptualization, F.S. and N.H.; methodology, N.H., S.A. and I.A.A.; software, A.A.; validation, A.A., M.A. and I.A.A.; formal analysis, M.A.; investigation, N.H., I.A.A. and F.S.; resources, F.S.; data curation, M.A.; writing—original draft preparation, F.S.; writing—review and editing, N.H., A.A. and S.A.; visualization, F.S.; supervision, F.S.; project administration, F.S.; funding acquisition, F.S. All authors have read and agreed to the published version of the manuscript.

Funding: This research project was supported by Researchers Supporting Project number (RSPD2023R1040), King Saud University, Riyadh, Saudi Arabia.

Institutional Review Board Statement: Not applicable.

Informed Consent Statement: Not applicable.

Data Availability Statement: The data are available on reasonable request from the corresponding author.

Acknowledgments: The authors are grateful to the Researchers Supporting Project number (RSPD2023R1040), King Saud University, Riyadh, Saudi Arabia for supporting this work.

Conflicts of Interest: The authors declare no conflict of interest.

Sample Availability: Samples of the compound ITN are available from the authors.

References

1. Berbenni, V.; Marini, A.; Bruni, G.; Cardini, A. Thermoanalytical and spectroscopic characterization of solid-state retinoic acid. *Int. J. Pharm.* **2001**, *221*, 123–141. [[CrossRef](#)]
2. Ghorab, M.M.; Babiker, M.E. Formulation and in-vitro evaluation of isotretinoin tablets. *J. Chem. Pharm. Res.* **2012**, *4*, 2817–2831.
3. Ascenso, A.; Guedes, R.; Bernardino, R.; Diogo, H.; Carvalho, F.A.; Santos, N.C.; Silva, A.M.; Marques, H.C. Complexation and full characterization of the tretinoin and dimethyl- β -cyclodextrin complex. *AAPS PharmSciTech* **2011**, *12*, 553–563. [[CrossRef](#)] [[PubMed](#)]
4. Muccio, D.D.; Brouillette, W.J.; Alam, M.; Vaezi, M.F.; Sani, B.P.; Venepally, P.; Reddy, L.; Li, E.; Norris, A.W.; Simpson-Herren, L.; et al. Conformationally defined 6-*s-trans*-retinoic acid analogs. 3. Structure–activity relationships for nuclear receptor binding, transcriptional activity, and cancer chemopreventive activity. *J. Med. Chem.* **1996**, *39*, 3625–3635. [[CrossRef](#)]
5. Muccio, D.D.; Brouillette, W.J.; Breritman, T.R.; Taimi, M.; Emanuel, P.D.; Zhang, X.; Chen, G.; Sani, B.P.; Venepally, P.; Reddy, L.; et al. Conformationally defined retinoic acid analogues. 4. Potential new agents for acute promyelocytic and juvenile myelomonocytic leukemias. *J. Med. Chem.* **1998**, *41*, 1679–1687. [[CrossRef](#)]
6. Levin, A.H.; Bos, M.E.; Zusi, F.C.; Nair, X.; Whiting, G.; Bouquin, P.; Tetrault, G.; Carrol, F.I. Evaluation of retinoids as therapeutic agents in dermatology. *Pharm. Res.* **1994**, *11*, 192–200.
7. Anadolu, R.Y.; Sen, T.; Tarimci, N.; Birol, A.; Erdem, C. Improved efficacy and tolerability of retinoic acid in acne vulgaris: A new topical formulation with cyclodextrin complex. *Eur. J. Acad. Dermatol. Venereol.* **2004**, *18*, 416–421. [[CrossRef](#)]
8. Loveday, S.M.; Singh, H. Recent advances in technologies for vitamin A protection in foods. *Trends Food Sci. Technol.* **2008**, *19*, 657–668. [[CrossRef](#)]
9. Gollnick, H.; Zouboulis, C.C. Not all acne is acne vulgaris. *Dtsch. Aerztebl. Int.* **2014**, *111*, 301–312. [[CrossRef](#)]
10. Espinosa, N.I.; Cohen, P.R. Acne vulgaris: A patient and physician’s experience. *Dermatol. Ther.* **2020**, *10*, 1–14. [[CrossRef](#)] [[PubMed](#)]
11. Fallah, H.; Rademaker, M. Isotretinoin for acne vulgaris—An update on adverse effects and laboratory monitoring. *J. Dermatol. Treat.* **2022**, *33*, 2414–2424. [[CrossRef](#)] [[PubMed](#)]
12. Alwhaibi, A.; Alenazi, M.; Almadi, B.; Alotaibi, A.; Alshehri, S.M.; Shakeel, F. A practical method for oral administration of pediatric oncology patient: A case study of neuroblastoma. *J. Oncol. Pharm. Pract.* **2023**, *29*, 755–759. [[CrossRef](#)] [[PubMed](#)]
13. Tan, X.; Meltzer, N.; Lindebaum, S. Solid-state stability studies of 13-*cis*-retinoic acid and all-*trans*-retinoic acid using microcalorimetry and HPLC analysis. *Pharm. Res.* **1992**, *9*, 1203–1208. [[CrossRef](#)]
14. Yap, K.L.; Liu, X.; Thenmozhiyal, J.C.; Ho, P.C. Characterization of the 13-*cis*-retinoic acid/cyclodextrin inclusion complexes by phase solubility, photostability, physicochemical and computational analysis. *Eur. J. Pharm. Sci.* **2005**, *25*, 49–56. [[CrossRef](#)]
15. Di, L.; Fish, P.V.; Mano, T. Bridging solubility between drug discovery and development. *Drug Discov. Today* **2012**, *17*, 486–495. [[CrossRef](#)]
16. Rezaei, H.; Rahimpour, E.; Zhao, H.; Martinez, F.; Barzegar-Jalali, M.; Jouyban, A. Solubility of baclofen in some neat and mixed solvents at different temperatures. *J. Mol. Liq.* **2022**, *347*, E118352. [[CrossRef](#)]
17. Barrett, J.A.; Yang, W.; Skolnik, S.M.; Belliveau, L.M.; Patros, K.M. Discovery solubility measurement and assessment of small molecules with drug development in mind. *Drug Discov. Today* **2022**, *27*, 1315–1325. [[CrossRef](#)] [[PubMed](#)]
18. Soliman, M.E.; Adewumi, A.T.; Akawa, O.B.; Subair, T.I.; Okunlola, F.O.; Akinsuku, A.E.; Khan, S. Simulation models for prediction of bioavailability of medicinal drugs—the interface between experiment and computation. *AAPS PharmSciTech* **2022**, *23*, E86. [[CrossRef](#)]

19. Yadav, K.; Sachan, A.K.; Kumar, S.; Dubey, A. Techniques for increasing solubility: A review of conventional and new strategies. *Asian J. Pharm. Res. Dev.* **2022**, *10*, 144–153. [[CrossRef](#)]
20. Jouyban, A. Review of the cosolvency models for predicting drug solubility in solvent mixtures: An update. *J. Pharm. Pharm. Sci.* **2019**, *22*, 466–485. [[CrossRef](#)]
21. Bolla, G.; Nangia, A. Pharmaceutical cocrystals: Walking the talk. *Chem. Commun.* **2016**, *52*, 8342–8360. [[CrossRef](#)] [[PubMed](#)]
22. Bolla, G.; Sarma, B.; Nangia, A.K. Crystal engineering of pharmaceutical cocrystals in the discovery and development of improved drugs. *Chem. Rev.* **2022**, *122*, 11514–11603. [[CrossRef](#)] [[PubMed](#)]
23. Duggirala, N.K.; Perry, M.L.; Almarsson, O.; Zaworotko, M.J. Pharmaceutical cocrystals: Along with the path to improve medicines. *Chem. Commun.* **2016**, *52*, 640–655. [[CrossRef](#)] [[PubMed](#)]
24. Paus, R.; Hart, E.; Ji, Y.; Sadowski, G. Solubility and caloric properties of cinnarizine. *J. Chem. Eng. Data* **2015**, *60*, 2256–2261. [[CrossRef](#)]
25. Ruether, F.; Sadowski, G. Modeling the solubility of pharmaceuticals in pure solvents and solvent mixtures for drug process design. *J. Pharm. Sci.* **2009**, *98*, 4205–4215. [[CrossRef](#)]
26. Alyamani, M.; Alshehri, S.; Alam, P.; Wani, S.U.D.; Ghoneim, M.M.; Shakeel, F. Solubility and solution thermodynamics of raloxifene hydrochloride in various (DMSO + water) compositions. *Alexand. Eng. J.* **2022**, *61*, 9119–9128. [[CrossRef](#)]
27. Guimarães, C.A.; Mena, F.; Mena, B.; Quenca-Guillena, J.S.; Matos, J.D.R.; Mercuri, L.P.; Braz, A.B.; Rossetti, F.C.; Kedor-Hackmann, E.R.M.; Santoro, M.I.R.M. Comparative physical–chemical characterization of encapsulated lipid-based isotretinoin products assessed by particle size distribution and thermal behavior analyses. *Thermochim. Acta* **2010**, *505*, 73–78. [[CrossRef](#)]
28. Patel, M.R.; Patel, R.B.; Parikh, J.R.; Patel, B.G. HPTLC method for estimation of isotretinoin in topical formulations, equilibrium solubility screening, and in vitro permeation study. *J. Liq. Chromatogr. Relat. Technol.* **2011**, *34*, 1783–1799. [[CrossRef](#)]
29. Patel, M.R.; Patel, R.B.; Parikh, J.R.; Patel, B.G. Improving the isotretinoin photostability by incorporating in microemulsion matrix. *ISRN Pharm.* **2011**, *2011*, E838016. [[CrossRef](#)]
30. Patel, M.R.; Patel, R.B.; Parikh, J.R.; Patel, B.G. Novel isotretinoin microemulsion-based gel for targeted topical therapy of acne: Formulation consideration, skin retention and skin irritation studies. *Appl. Nanosci.* **2016**, *6*, 539–553. [[CrossRef](#)]
31. Chavda, H.; Patel, J.; Chavada, D.; Dave, S.; Patel, A.; Patel, C. Self-nanoemulsifying powder of isotretinoin: Preparation and characterization. *J. Powder Technol.* **2013**, *2013*, E108569. [[CrossRef](#)]
32. Hosny, K.M.; Al Nahyah, K.S.; Alhakamy, N.A. Self-nanoemulsion loaded with a combination of isotretinoin, an antiacne drug, and quercetin: Preparation, optimization, and in vivo assessment. *Pharmaceutics* **2021**, *13*, 46. [[CrossRef](#)] [[PubMed](#)]
33. Shakeel, F.; Haq, N.; Mahdi, W.A.; Alsarra, I.A.; Alshehri, S.; Alenazi, M.; Alwhaibi, A. Solubilization and thermodynamic analysis of isotretinoin in eleven different green solvents at different temperatures. *Materials* **2023**, *15*, 8274. [[CrossRef](#)] [[PubMed](#)]
34. Alsenz, J.; Kansy, M. High throughput solubility measurement in drug discovery and development. *Adv. Drug Deliv. Rev.* **2007**, *59*, 546–567. [[CrossRef](#)]
35. Wernersson, S.; Birgersson, S.; Akke, M. Cosolvent dimethyl sulfoxide influences protein–ligand binding kinetics via solvent viscosity effects: Revealing the success rate of complex formation following diffusive protein–ligand encounter. *Biochemistry* **2023**, *62*, 44–52. [[CrossRef](#)]
36. Novales, N.A.; Schwans, J.P. Comparing the effects of organic cosolvents on acetylcholinesterase and butyrylcholinesterase activity. *Anal. Biochem.* **2022**, *654*, E114796. [[CrossRef](#)]
37. Stenstrom, O.; Diehl, C.; Modig, K.; Nilsson, U.J.; Akke, M. Mapping the energy landscape of protein–ligand binding via linear free energy relationships determined by protein NMR relaxation dispersion. *RSC Chem. Biol.* **2021**, *2*, 259–265. [[CrossRef](#)]
38. Shakeel, F.; Haq, N.; Salem-Bekhit, M.M.; Raish, M. Solubility and dissolution thermodynamics of sinapic acid in (DMSO + water) binary solvent mixtures at different temperatures. *J. Mol. Liq.* **2017**, *225*, 833–839. [[CrossRef](#)]
39. Shakeel, F.; Alshehri, S.; Imran, M.; Haq, N.; Alanazi, A.; Anwer, M.K. Experimental and computational approaches for solubility measurement of pyridazinone derivative in binary (DMSO + water) systems. *Molecules* **2019**, *25*, 171. [[CrossRef](#)]
40. Alshahrani, S.M.; Shakeel, F. Solubility data and computational modeling of baricitinib in various (DMSO + water) mixtures. *Molecules* **2020**, *26*, 2124. [[CrossRef](#)]
41. Tinjaca, D.A.; Martinez, F.; Almanza, O.A.; Pena, M.A.; Jouyban, A.; Acree, W.E., Jr. Increasing the equilibrium solubility of meloxicam in aqueous media by using dimethyl sulfoxide as a cosolvent: Correlation, dissolution thermodynamics and preferential solvation. *Liquids* **2022**, *2*, 161–182. [[CrossRef](#)]
42. Yao, X.; Wang, Z.; Geng, Y.; Zhao, H.; Rahimpour, E.; Acree, W.E., Jr.; Jouyban, A. Hirshfeld surface and electrostatic potential surface analysis of clozapine and its solubility and molecular interactions in aqueous blends. *J. Mol. Liq.* **2022**, *360*, E119328. [[CrossRef](#)]
43. Zhang, Y.; Shi, X.; Yu, Y.; Zhao, S.; Song, H.; Chen, A.; Shang, Z. Preparation and characterization of vanillin cross-linked chitosan microspheres of pterostilbene. *Int. J. Polym. Anal. Charact.* **2014**, *19*, 83–93. [[CrossRef](#)]
44. Mohammadian, E.; Rahimpour, E.; Martinez, F.; Jouyban, A. Budesonide solubility in polyethylene glycol 400+ water at different temperatures: Experimental measurement and mathematical modelling. *J. Mol. Liq.* **2019**, *274*, 418–425. [[CrossRef](#)]
45. Apelblat, A.; Manzurola, E. Solubilities of o-acetylsalicylic, 4-aminosalicylic, 3,5-dinitrosalicylic and p-toluic acid and magnesium-DL-aspartate in water from T = (278–348) K. *J. Chem. Thermodyn.* **1999**, *31*, 85–91. [[CrossRef](#)]

46. Manzurola, E.; Apelblat, A. Solubilities of L-glutamic acid, 3-nitrobenzoic acid, acetylsalicylic, p-toluic acid, calcium-L-lactate, calcium gluconate, magnesium-DL-aspartate, and magnesium-L-lactate in water. *J. Chem. Thermodyn.* **2002**, *34*, 1127–1136. [[CrossRef](#)]
47. Ksiazczak, A.; Moorthi, K.; Nagata, I. Solid-solid transition and solubility of even n-alkanes. *Fluid Phase Equilib.* **1994**, *95*, 15–29. [[CrossRef](#)]
48. Tong, Y.; Wang, Z.; Yang, E.; Pan, B.; Jiang, J.; Dang, P.; Wei, H. Determination and correlation of solubility and solution thermodynamics of ethenzamide in different pure solvents. *Fluid Phase Equilib.* **2016**, *427*, 549–556. [[CrossRef](#)]
49. Shakeel, F.; Alshehri, S. Solubilization, Hansen solubility parameters, solution thermodynamics and solvation behavior of flufenamic acid in (Carbitol + water) mixtures. *Processes* **2020**, *8*, 1204. [[CrossRef](#)]
50. Yalkowsky, S.H.; Roseman, T.J. Solubilization of drugs by cosolvents. In *Techniques of Solubilization of Drugs*; Yalkowsky, S.H., Ed.; Marcel Dekker Inc.: New York, NY, USA, 1981; pp. 91–134.
51. Jouyban, A.; Acree, W.E., Jr. Mathematical derivation of the Jouyban-Acree model to represent solute solubility data in mixed solvents at various temperatures. *J. Mol. Liq.* **2018**, *256*, 541–547. [[CrossRef](#)]
52. Higuchi, T.; Connors, K.A. Phase-solubility techniques. *Adv. Anal. Chem. Instr.* **1965**, *4*, 117–122.
53. Haq, N.; Alshehri, S.; Alsarra, I.A.; Alenazi, M.; Alwhaibi, A.; Shakeel, F. Environmentally friendly stability-indicating HPLC method for the determination of isotretinoin in commercial products and solubility samples. *Heliyon* **2023**, *9*, E18405. [[CrossRef](#)] [[PubMed](#)]
54. Zhu, Q.N.; Wang, Q.; Hu, Y.B.; Abliz, X. Practical determination of the solubility parameters of 1-alkyl-3-methylimidazolium bromide ([CnClm]Br, n = 5, 6, 7, 8) ionic liquids by inverse gas chromatography and the Hansen solubility parameter. *Molecules* **2019**, *24*, 1346. [[CrossRef](#)] [[PubMed](#)]
55. Wan, Y.; He, H.; Huang, Z.; Zhang, P.; Sha, J.; Li, T.; Ren, B. Solubility, thermodynamic modeling and Hansen solubility parameter of 5-norbornene-2,3-dicarboximide in three binary solvents (methanol, ethanol, ethyl acetate + DMF) from 278.15 K to 323.15 K. *J. Mol. Liq.* **2020**, *300*, E112097. [[CrossRef](#)]
56. Ruidiaz, M.A.; Delgado, D.R.; Martínez, F.; Marcus, Y. Solubility and preferential solvation of indomethacin in 1,4-dioxane + water solvent mixtures. *Fluid Phase Equilib.* **2010**, *299*, 259–265. [[CrossRef](#)]
57. Hildebrand, J.H.; Prausnitz, J.M.; Scott, R.L. *Regular and Related Solutions*; Van Nostrand Reinhold: New York, NY, USA, 1970.
58. Manrique, Y.J.; Pacheco, D.P.; Martínez, F. Thermodynamics of mixing and solvation of ibuprofen and naproxen in propylene glycol + water cosolvent mixtures. *J. Sol. Chem.* **2008**, *37*, 165–181. [[CrossRef](#)]
59. Shakeel, F.; Bhat, M.A.; Haq, N.; Fathi-Azarbayjani, A.; Jouyban, A. Solubility and thermodynamic parameters of a novel anti-cancer drug (DHP-5) in polyethylene glycol 400 + water mixtures. *J. Mol. Liq.* **2017**, *229*, 241–245. [[CrossRef](#)]
60. Cong, Y.; Du, C.; Xing, K.; Bian, Y.; Li, X.; Wang, M. Research on dissolution of actarit in aqueous mixtures: Solubility determination and correlation, preferential solvation, solvent effect and thermodynamics. *J. Mol. Liq.* **2022**, *355*, E119141. [[CrossRef](#)]
61. Tinjaca, D.A.; Martinez, F.; Almanza, O.A.; Jouyban, A.; Acree, W.E., Jr. Solubility, correlation, dissolution thermodynamics and preferential solvation of meloxicam in aqueous mixtures of 2-propanol. *Pharm. Sci.* **2022**, *28*, 130–144. [[CrossRef](#)]
62. Krug, R.R.; Hunter, W.G.; Grieger, R.S. Enthalpy-entropy compensation. 2. Separation of the chemical from the statistic effect. *J. Phys. Chem.* **1976**, *80*, 2341–2351. [[CrossRef](#)]
63. Holguín, A.R.; Rodríguez, G.A.; Cristancho, D.M.; Delgado, D.R.; Martínez, F. Solution thermodynamics of indomethacin in propylene glycol + water mixtures. *Fluid Phase Equilib.* **2012**, *314*, 134–139. [[CrossRef](#)]
64. Behboudi, E.; Soleymani, J.; Martinez, F.; Jouyban, A. Solubility of amlodipine besylate in binary mixtures of polyethylene glycol 400 + water at various temperatures: Measurement and modelling. *J. Mol. Liq.* **2022**, *347*, E118394. [[CrossRef](#)]
65. Mohammadian, E.; Foroumadi, A.; Hasanvand, Z.; Rahimpour, E.; Zhao, H.; Jouyban, A. Simulation of mesalazine solubility in the binary solvents at various temperatures. *J. Mol. Liq.* **2022**, *357*, E119160. [[CrossRef](#)]

Disclaimer/Publisher's Note: The statements, opinions and data contained in all publications are solely those of the individual author(s) and contributor(s) and not of MDPI and/or the editor(s). MDPI and/or the editor(s) disclaim responsibility for any injury to people or property resulting from any ideas, methods, instructions or products referred to in the content.